A Numerical Study of Force-Based Boundary Conditions in Multiparticle Collision Dynamics

Arturo Ayala-Hernandez, Humberto Híjar

Abstract—We propose a new alternative method for imposing fluid-solid boundary conditions in simulations of Multiparticle Collision Dynamics. Our method is based on the introduction of an explicit potential force acting between the fluid particles and a surface representing a solid boundary. We show that our method can be used in simulations of plane Poiseuille flows. Important quantities characterizing the flow and the fluid-solid interaction like the slip coefficient at the solid boundary and the effective viscosity of the fluid, are measured in terms of the set of independent parameters defining the numerical implementation. We find that our method can be used to simulate the correct hydrodynamic flow within a wide range of values of these parameters.

Keywords—Multiparticle Collision Dynamics, Fluid-Solid Boundary Conditions, Molecular Dynamics.

I. INTRODUCTION

MULTIPARTICLE Collision Dynamics (MPC) is a recent numerical technique originally proposed by Malevanets and Kapral [1], [2], which has turned out to be a very attractive procedure for studying diverse systems of soft condensed matter. It represents a particle-based method, a feature that makes it suitable for using it in combination with Molecular Dynamics (MD) [3] in the study of complex systems, e.g. colloidal suspensions and polymer solutions. In a typical MD-MPC simulation, the evolution of the suspended particles is followed at the microscopic level by using MD, while MPC provides a simplified coarse-grained description for the solvent. This kind of hybrid algorithm is used to bridge the characteristic gaps in time, length and energy existing in the dynamics of the afore mentioned systems [2], [4]–[6]. It has been shown that MPC captures correctly the hydrodynamic behavior of the fluid around the embedded particles and yields the correct hydrodynamic interactions existing between them [6]. In addition, MPC has a stochastic character giving rise to hydrodynamic fluctuations and to random Brownian forces on the suspended particles [6], [7]. Thus, fluids simulated via MPC can be used as thermal baths supporting also hydrodynamic interactions.

Two of the main advantages offered by MPC are the relative simplicity of its algorithm and its stability over long-time simulations. Remarkably, it has been possible to characterize MPC also from the analytical point of view, by calculating closed expressions for the transport coefficients of MPC fluids in terms of the parameters defining the simulations.

Grupo de Sistemas Inteligentes, Facultad de Ingeniería. Universidad La Salle, Benjamin Franklin 47, 06140, D.F. México.
Corresponding author: H. Híjar. Also at SNI, Mexico.
E-mail addresses: humberto.hijar@lasallistas.org.mx (H. Híjar), and kudramh@gmail.com (A. Ayala-Hernandez).

For the original version of MPC, commonly refereed as Stochastic Rotation Dynamics (SRD), explicit analytical expressions for the viscosity and the thermal conductivity have been obtained from both a discrete-time projection operator techniques [8]–[10], and from a kinetic theory approach [11]. More recently, the corresponding analytical expressions for the viscosities have been also obtained for variations of the original SRD algorithm [12]. In all these cases simulation results have been found to agree very well with the analytical expressions, thus demonstrating that an excellent analytical description and understanding of MPC has been achieved.

Up to now, MPC has been used for simulating systems as diverse as colloids [2], [6] and suspensions of polymers [13], polymers under flow [7], [14], [15], flow around objects [16], [17], vesicles under flow [18], particle sedimentation [19], [20], backtracking of colloidal particles [21], and tracking control of colloidal particles in fluids under steady flows [22].

Diverse boundary conditions have been used in the literature of the subject in order to impose constraints on the motion of fluids simulated via MPC. An analysis of the effects that these boundary conditions have on the dynamics of MPC fluids has been carried out in [23]. There, however, all the studied cases correspond to boundary conditions imposed by so-called *hard walls*, i.e. walls that confine the fluid by simply reflecting the incoming particles back into the bulk system. The interaction of the MPC fluid with reflecting walls introduces modifications in the stress tensor that have been calculated for confinement in a slit geometry in [24]. There, a properly modified form of the MPC algorithm in the presence of walls has been proposed that prevents any surface slip of the confined particles and allows for simulating the correct plane Couette velocity profile.

In the present work we propose a new method that can be used to simulate MPC fluids confined by solid walls. Our approach consists in introducing explicit repulsive forces which restrict the motion of the MPC particles within specific regions of the space. These forces are derived by assuming that the physical walls that constrain the motion of the fluid are constituted by a continuous surface distributions of particles. In order to check the validity of the proposed method, we consider its performance in simulations of MPC fluids confined between two parallel planes and in the presence of a uniform pressure gradient (plane Poiseuille flow). We show that our method allows for reproducing the correct velocity profile expected for a viscous fluid under such conditions. Our paper is organized as follows. In Section II we derive the expression for the confinement force to be used in our simulations. In Section III we discuss the details about the

implementation of the method. Then, in Section IV we present the results obtained for the simulation of flow between parallel plates induced by a uniform pressure gradient. In Section V we summarize our main conclusions, discuss some advantages of our approach and state its limitations.

II. CONFINEMENT FORCES

A. Fluid-Solid Interaction

Let us consider an ensemble of particles moving through a channel or pore defined by a wall with irregular geometry, as it is schematically illustrated in Fig. 1a. In order to confine the particles inside the pore, we will assume that the latter consists of a continuous surface distribution of particles, which interact with the confined particles via a generalized Weeks-Chandler-Andersen (WCA) potential. Thus, if $\vec{R}$ and $\vec{R}'$ denote the position vectors of a confined and a surface particle, respectively, their interaction will be given by [25]

$$\phi\left(\vec{R}, \vec{R}'\right) = \epsilon \left[\left(\frac{\sigma}{\left|\vec{R} - \vec{R}'\right|} \right)^{12n} - \left(\frac{\sigma}{\left|\vec{R} - \vec{R}'\right|} \right)^{6n} + \frac{1}{4} \right],$$
(1)

if $\left|\vec{R} - \vec{R}'\right| < \tilde{\sigma}$; and will be zero if $\left|\vec{R} - \vec{R}'\right| \geq \tilde{\sigma}$. In (1), ϵ is the interaction strength, σ is the effective diameter of the interaction, n is a positive integer, and $\tilde{\sigma} = 2^{\frac{1}{6n}} \sigma$ is the cutoff radius of the interaction.

Let ρ_S denote the numerical surface density of particles at the wall, which hereafter will be assumed to be uniform. Then, the total potential at the position $\vec{R}$ inside the pore will be

$$\Phi\left(\vec{R}\right) = \rho_S \int_{S^*} dS' \phi\left(\vec{R}, \vec{R}'\right),$$
(2)

where S^* denotes the set of all those points at the surface which satisfy the condition $\left|\vec{R} - \vec{R}'\right| < \tilde{\sigma}$.

For particles located at positions $\vec{R}'$ in which the right hand side of (2) does not vanish, we will approximate the integral by its mean value. This procedure yields

$$\Phi\left(\vec{R}\right) \simeq \rho_S S^* \phi\left(\vec{R}, \vec{R}^*\right),$$
(3)

where $\vec{R}^*$ is the closest point of the surface to the position $\vec{R}$, see Fig. 1 **a**.

In the present work we will only consider the limiting case in which the size of the confined particles is small as compared with the characteristic dimensions of the confining wall. In this limit the curvature of the surface is not significant and S^* can be approximated at first order as the cross section corresponding to the intersection of a solid sphere of radius $\tilde{\sigma}/2$ with a plane located at a distance $\left|\vec{R} - \vec{R}^*\right|/2$ from its center, i.e.

$$S^* \simeq \frac{\pi}{4} \left(\tilde{\sigma}^2 - \left|\vec{R} - \vec{R}^*\right|^2 \right).$$
(4)

Replacing (4) into (3) yields the expression for the interaction potential between the surface and the confined particles,

$$\Phi\left(\vec{R}\right) = \frac{\pi \epsilon \rho_S}{4} \left(\tilde{\sigma}^2 - \left|\vec{R} - \vec{R}^*\right|^2 \right) \left[\left(\frac{\sigma}{\left|\vec{R} - \vec{R}^*\right|} \right)^{12n} - \left(\frac{\sigma}{\left|\vec{R} - \vec{R}^*\right|} \right)^{6n} + \frac{1}{4} \right],$$
(5)

which is valid if $\left|\vec{R} - \vec{R}^*\right| < \tilde{\sigma}$; while $\Phi\left(\vec{R}\right) = 0$, if $\left|\vec{R} - \vec{R}^*\right| \geq \tilde{\sigma}$.

In the previous expression, $\vec{R}^*$ is indeed a function of $\vec{R}$ which must be given in order to obtain the explicit form of the potential Φ. The specific dependence of $\vec{R}^*$ on $\vec{R}$ is determined from the geometry of the pore.

At this point let us simply assume that the function $\vec{R}^*\left(\vec{R}\right)$ is known. Thus, we can calculate the force exerted by the pore on a particle located at position $\vec{R}$. Since Φ depends on $\vec{R}$ only through the quantity $|\vec{R} - \vec{R}^*|^2$, this force is giving by

$$\vec{F}\left(\vec{R}\right) = -\vec{\nabla}\Phi = -2 \frac{d\Phi}{d|\vec{R} - \vec{R}^*|^2} \left(\vec{R} - \vec{R}^*\right).$$
(6)

Now, by calculating the derivative of Φ with respect to $|\vec{R} - \vec{R}^*|^2$ explicitly, we obtain

$$\vec{F}\left(\vec{R}\right) = \frac{\pi \epsilon \rho_S}{2} \left(\vec{R} - \vec{R}^*\right) \left\{ 3n \frac{\tilde{\sigma}^2 - |\vec{R} - \vec{R}^*|^2}{\sigma^2} \right.$$
$$\left[2 \left(\frac{\sigma}{|\vec{R} - \vec{R}^*|} \right)^{12n+2} - \left(\frac{\sigma}{|\vec{R} - \vec{R}^*|} \right)^{6n+2} \right]$$
$$\left. + \left[\left(\frac{\sigma}{|\vec{R} - \vec{R}^*|} \right)^{12n} - \left(\frac{\sigma}{|\vec{R} - \vec{R}^*|} \right)^{6n} + \frac{1}{4} \right] \right\},$$
(7)

when $\left|\vec{R} - \vec{R}^*\right| < \tilde{\sigma}$; while the force vanishes for particles such that $\left|\vec{R} - \vec{R}^*\right| \geq \tilde{\sigma}$. It can be noticed that $\vec{F}\left(\vec{R}\right)$ is indeed a continuous vector field, which points along the vector $\vec{R} - \vec{R}^*$ for particles close to the surface of the pore.

As it was mentioned above, in order to obtain closed expressions for $\Phi\left(\vec{R}\right)$ and $\vec{F}\left(\vec{R}\right)$, an analytical function for $\vec{R}^*$ in terms of $\vec{R}$ must be given. As it can be anticipated, this can be done only for a very reduced number of confining surfaces. Among them, one important case is the one corresponding to a plane defined by the equation $x = x_0$, with x_0 a constant. This is the case illustrated in Fig. 1 **b**, where we clearly have

$$\vec{R}^* = \vec{R} - (x - x_0)\hat{e}_x,$$
(8)

with $\hat{e}_x$ denoting the unitary vector along the x direction. Thus, by replacing the previous expression into (7), the explicit form

of $\vec{F}$ can be found in terms $\vec{R}$ only. Specifically,

$$
\begin{aligned}
\vec{F}\left(\vec{R}\right) = {} & (x - x_o)\,\hat{e}_x \frac{\pi\epsilon\rho_S}{2}\left\{3n\frac{\tilde{\sigma}^2 - |x - x_o|^2}{\sigma^2}\right. \qquad (9)\\
& \left[2\left(\frac{\sigma}{|x - x_o|}\right)^{12n+2} - \left(\frac{\sigma}{|x - x_o|}\right)^{6n+2}\right]\\
& \left.+\left[\left(\frac{\sigma}{|x - x_o|}\right)^{12n} - \left(\frac{\sigma}{|x - x_o|}\right)^{6n} + \frac{1}{4}\right]\right\},
\end{aligned}
$$

if $|x - x_o| < \tilde{\sigma}$, and 0 if $|x - x_o| \geq \tilde{\sigma}$.

In the present paper we shall restrict our analysis to the case of a MPC fluid restricted to move in the space between two parallel planes. Consequently, we will use (9) for achieving the corresponding confinement force.

It should be stressed, however, that (9) gives rise to purely repulsive forces between the solid surface and the confined particles. These forces point along the normal direction to the confining surface. Accordingly, the incoming particles colliding with the surface will be reflected back into the bulk system and only the normal component of their momentum will be reversed. Thus, only slip boundary conditions can be obtained from the direct application of (9), and it can not be used to simulate rough surfaces.

In order to generalize our formalism and to make it able to simulate the effects produced by uneven surfaces, we will propose a modification in the application of (9), in which the magnitude of the force is preserved, but its direction is taken along the unit vector $\hat{v}_{\text{in}} = -\vec{v}/v$, where $\vec{v}$ represents the velocity with which the particle hits the confining wall.

Therefore, the confining force on a fluid particle will act along the direction in which it penetrates the surface. In the following section we will analyze the effects that the application of the proposed confinement force has on the dynamics of an ensemble of MPC particles.

B. Wall Stress Tensor

For the system described in subsection II-A, confinement of the fluid is achieved by incorporating a direct interaction of its constituting particles with a wall. The momentum exchange resulting from this interaction produces a kinetic contribution to the stress tensor of the fluid. In order to simplify the calculation of the stress tensor contribution arising from collisions with the surface, we shall restrict ourselves to consider the situation described by (9), in which the confining surface is a plane parallel to the y-z plane. Moreover, in order simplify further the involved mathematical analysis, we shall make the additional assumption of considering that the force experienced by the fluid particle when it penetrates the wall is uniform and can be approximated in terms of an effective constant force field of magnitude F_{e}. Thus, let us consider a time interval from t_q to $t_q + h$, and a particle with initial velocity $\vec{v}(t_q)$ that collides with the wall at time $t_q + \Delta t$, with $\Delta t < h$. The change in the momentum of this particle due to its interaction with the wall is found to be

$$
\Delta\vec{p}^{\,\text{w}} = -(h - \Delta t)\,F_{\text{e}}\frac{\vec{v}(t_q - \Delta t)}{v(t_q - \Delta t)}. \qquad (10)
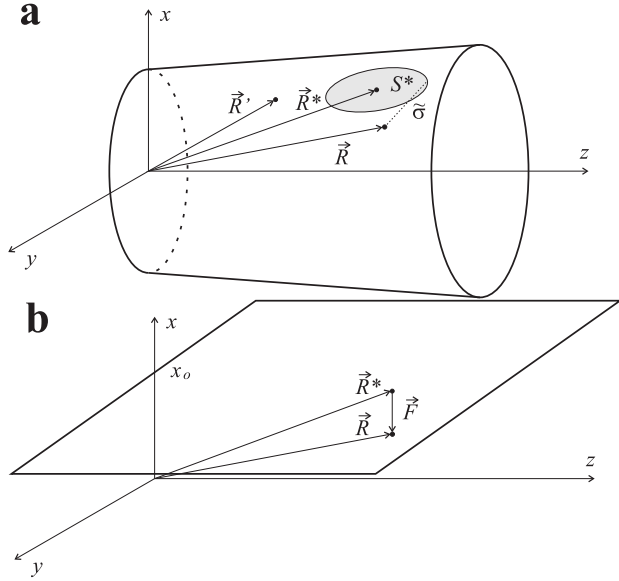$$

Fig. 1. **a** Auxiliary quantities used to derive the force exerted by a solid boundary on a confined fluid. Vectors $\vec{R}$, $\vec{R}'$ and $\vec{R}*$, represent, respectively, the position of a particle in the system, the position of a surface particle and the closest point of the surface to the vector $\vec{R}$. The area $S*$ and the distance $\tilde{\sigma}$ are defined through the text. **b** Special case of a plane confining wall.

Then, the total momentum per unit time per unit area exchanged with the wall by all the particles having the same initial velocity can be written in the form

$$
\Delta\vec{\Xi} = -F_{\text{e}}\rho_{\text{f}}hv_x(t_q)\left(1 - \frac{\tilde{x}(t_q)}{hv_x(t_q)}\right)\frac{\vec{v}(t_q - \Delta t)}{v(t_q - \Delta t)}, \qquad (11)
$$

where ρ_{f} denotes the numerical density of fluid particles and $\tilde{x}(t_q)$ is initial distance to the wall in the x-direction.

We will consider now the presence of a uniform external force per unit mass, $\vec{g}$, which may play the role of a pressure gradient acting on the confined fluid. We thus have $\vec{v}(t_q + \Delta t) = \vec{v}(t_q) + \Delta t\vec{g}$. It should be stressed that in the present work we shall restrict ourselves to consider only small values of g, and assume that fluid particles are uniformly distributed in space. Then, by expanding the right hand side of (11) in a Taylor up to first order in $\vec{g}$, and averaging over the initial positions we obtain the following expression for the xz component of the stress tensor

$$
\sigma_{xz} = -\frac{\rho_{\text{f}}h^2v_x^2F_{\text{e}}}{2L_xv}\left[v_z + \frac{gh}{3}\left(1 - \frac{v_z^2}{v^2}\right)\right], \qquad (12)
$$

where all velocities are evaluated at the initial time t_q.

Equation (12) shows that the proposed confining force is expected to produce a stress tensor contribution at the wall that is independent of the external force and a term increasing linearly with g, for small values of this quantity. The former contribution will introduce an apparent viscosity at the wall that will produce slip boundary conditions. On the other hand, higher order terms on g that have not been considered in (12) will produce non-Newtonian effects by making the viscosity of the confined fluid to depend on the externally applied force. This effects, however, are not expected to be significant if g is kept small.

III. SIMULATIONS OF PLANE POISEUILLE FLOW IN MPC FLUIDS

A. Hybrid MD-MPC Algorithm with Confining Walls

In order to test the performance of the previous model, we conduct a series of simulations of Poiseuille flow confined between two parallel planes. A well-known analytical solution for the flow profile exists in this case, which serves as a clear test of the accuracy of the algorithm. The location of the planes is defined by the equations $x = L_x/2$, and $x = -L_x/2$, where L_x denotes the distance between the planes. The lengths of the planes along the y and z directions are L_y and L_z, respectively, where $L_y, L_z \gg L_x$. The planes will be assumed to be constituted by a continuous distribution of particles with surface density ρ_S.

The confined MPC fluid will be assumed to be an ensemble of N particles of mass m, whose positions and velocities are continuous functions of the time t. An external uniform field will be considered to be present which exerts a force per unit mass $\vec{g}$ on the fluid particles. For simplicity, $\vec{g}$ will be assumed to point along the z-axis, i.e. $\vec{g} = g\hat{e}_z$.

The time evolution of the system will be simulated by means of a hybrid technique combining MD and MPC. On the one hand, MD will allow us to simulate the behavior of the particles at the microscopic time-scale and will take care of the interaction of the fluid particles with the confining walls. On the other hand, MPC will consider the interaction between the fluid particles in coarse-grained scheme and will allow us to incorporate the effects occurring at the hydrodynamic time-scales.

The simulation will proceed in two main steps. In the first one, the positions and velocities of the MPC particles will be updated according to the velocity Verlet algorithm, i.e.

$$\vec{R}_i(t + \Delta t) = \vec{R}_i(t) + \Delta t \vec{v}_i(t) + \frac{(\Delta t)^2}{2m}\vec{F}_i(t), \qquad (13)$$

and

$$\vec{u}_i(t + \Delta t) = \vec{u}_i(t) + \frac{\Delta t}{2m}\left[\vec{F}_i(t + \Delta t) + \vec{F}_i(t)\right], \qquad (14)$$

for $i = 1, 2, \ldots, N$. In the previous expressions $\vec{R}_i$ and $\vec{v}_i$ are the position and velocity vectors of the i-th fluid particle; and Δt represents the microscopic time-step of the MD method. Notice in addition that $\vec{F}_i$ denotes the total force field acting on the i-th particle, which must be calculated by adding the confining force given by (9), and the external force field $m\vec{g}$.

The second main step of the simulation algorithm is precisely the so-called collision step of the MPC method. In this step, the simulation box is subdivided into cells of volume a^3, forming an evenly spaced grid, and interparticle collisions are simulated by various momentum swapping schemes within each cell. The center-of-mass velocity of each cell is calculated according to

$$\vec{u}_\mu(t) = \frac{1}{N_\mu}\sum_{i \in \mu}\vec{v}_i(t), \qquad (15)$$

where the Greek index μ has been used to indicate the μ-th cell and N_μ represents the total number of particles in that cell. Finally, particles located in the same cell are forced to collide according to the SRD rule

$$\vec{v}_i(t + \Delta t) = \vec{u}_\mu(t) + \mathbf{R}(\alpha; \vec{n}_\mu(t)) \cdot [\vec{v}_i(t) - \vec{u}_\mu(t)]. \quad (16)$$

Here μ indicates the cell where the i-th particle is located and $\mathbf{R}$ is a stochastic rotation matrix which rotates velocities by a fixed angle α around a random axis $\vec{n}_\mu$. In our simulations, the vector $\vec{n}_\mu$ is produced in each cell at every time-step by randomly selecting a point on the surface of a sphere with unit radius.

It should be stressed that the collision rule described by (15) and (16) is not applied every time-step but at intervals of time of size $\Delta t_{\text{MPC}} = \tilde{n}\Delta t$, where $\tilde{n}$ is a positive integer.

In the hybrid algorithm discussed so far, the presence of collision cells introduces an artificially fixed frame of reference, which breaks Galilean invariance, leading to a breakdown of the molecular chaos assumption. In order to restore this property, a random displacement of the collision cells is produced before collisions take place. This random displacement procedure has important implications for various aspects of MPC simulations due to the presence of solid planes. Without the random displacement, the boundary cells coincides with the respective planes. When displacement occurs, an additional collision cell is added below the lower plane and the whole collision cells are displaced in the positive x-direction by a uniform vector with components uniformly distributed within the range $[-a/2, a/2]$.

The random displacement leads to partially occupied cells at the planes and virtual particles must be added to every partially empty cell cut off by the plane. In the present work we will follow a procedure similar to the one used in [24], where the number of virtual particles, N_{vp}, is determined by the number of fluid particles, N_{fp}, in the boundary cell cut off by the opposite plane. In this manner, the average particle density $\langle N_{vp} + N_{fp}\rangle = N_\mu$, is restored on partially empty cells. According to this procedure, the center of mass velocity of the particles in a boundary cell is

$$\vec{u}_\mu(t) = \frac{1}{m(N_{fp} + N_{vp})}\left(\sum_{i=1}^{N_{fp}} m\vec{v}_i(t) + \sum_{j=1}^{N_{vp}} m\vec{v}_j(t)\right). \qquad (17)$$

Collisions are executed and the total force on a fluid particle comprises contributions from collisions among particles and collisions with the planes. The momentum exchange between fluid and virtual particles at the boundary contributes to the stress tensor at the wall with a collision term, which is found to be [24]

$$\langle \Delta P_x \rangle = \frac{2(\cos \alpha - 1)m}{3N_c}\langle N_{fp}N_{vp}(\vec{u}_\mu - \vec{v}_p)\rangle. \qquad (18)$$

Here $\vec{v}_p$ represents the average velocity of virtual particles on the ensemble. It should be noted that this average vanish to zero at equilibrium. In order to ensure that virtual particles do not modify the stress tensor at the boundary wall we propose that the must be introduced with the average velocity of the N_{fp} particles on the opposite cell cut off by the plane. On the average, this procedure will cancel the momentum exchange

as it can be observed from (18), and the stress tensor will only have the kinetic contributions described previously by (12).

We consider periodic boundary conditions along the y and z Cartesian directions. In order to prevent heating of the simulated system due to the work performed by the confinement forces [26], we apply a thermostating procedure after each collision step which fixes the temperature of the system at a specific value T_0. With this purpose we consider a thermostat acting at the cell level such that relative velocities of the particles with respect to the center of mass velocity of the cell are rescaled by the factor $(T_0/T_\mu)^{1/2}$, where the local temperature field is defined by

$$T_\mu(t) = \frac{m}{3k_B(N_\mu - 1)} \sum_{i \in \mu} [\vec{v}_i(t) - \vec{u}_\mu(t)]. \quad (19)$$

The general schedule followed in performing simulations consisted of the following main parts. Firstly, particles were sorted into the simulation box with random positions and velocities taken from uniform distributions. No initial overlapping existed between the fluid particles and the confining surface, the total momentum of the system was fixed to zero, and its total energy was adjusted to the value dictated by the equipartition theorem. Then, the hybrid MD-MPC algorithm was applied to the ensemble of fluid particles subjected to the external field $\vec{g}$ and to the constraining surface forces. This thermalization precess was applied for a period of time large enough to guarantee that the proper distribution of velocities and hydrodynamic fields were established.

Finally, a long enough simulation stage was performed that allowed us to calculate the average velocity field established in the system.

B. Simulation Parameters

We chose the independent parameters defining our numerical implementation to be: the length of the MPC cells, a; the time-step between SRD collisions, Δt_{MPC}; the average number of particles per cell, N_p; the thermal energy, $k_B T_0$; the rotation angle for SRD, α; and the mass of the individual MPC particles, m. All our simulations were performed by fixing the following values: $a = 1$, $k_B T_0 = 1$, $N_p = 5$, $\Delta t_{\text{MPC}} = 0.05$, and $m = 1$. Notice that here, as well in the rest of the present work, simulation units (s.u.) will be used instead of physical units.

We considered a system with a volume defined by the quantities $L_x = 10a$, and $L_y = L_z = 20a$. On the other hand, the parameters characterizing the interaction between the particles and the confining walls were chosen as $\epsilon = 0.5k_B T_0$, $\sigma = 0.5a$, and $\rho_S = 2a^{-2}$. The MD time-step was chosen as $\Delta t = 0.005$, for which no instabilities of the simulations were observed.

Simulations were implemented in which the SRD collision angle α took twelve different values uniformly distributed within the range $[15°, 180°]$. Notice that for small values of the collision angle, the simulated system is expected to behave close to the so-called gas regime, in which kinetic contributions to the material properties dominate over collisional contributions. On the opposite case, for values of α close to $180°$, the dynamics of the simulated fluid is expected to be in the so-called liquid regime, where collisional effects are larger and dominate over kinetic effects. Thus, in our numerical experiments we were able to explore the complete range of behaviors expected in simulations of MPC fluids.

For the previously described set of parameters, we performed simulations in which the systems were allowed to thermalize in a total of 2×10^5 steps of the MD-MPC algorithm, while the evaluation of their average properties was performed through simulations extending along 4×10^5 simulation steps.

IV. RESULTS

A. Viscosity Estimation

The viscosity coefficient of the simulated MPC fluid was estimated experimentally as function of the collision angle α. With this purpose we noticed firstly that the velocity profile expected for a viscous fluid confined between two parallel planes and subjected to a parallel uniform force field per unit mass $\vec{g}$, is the classical Poiseuille flow [27], which will be cast in the form

$$v_z(x) = \frac{g}{2\nu} \left[\left(\frac{D_x}{2} \right)^2 - x^2 \right], \quad (20)$$

where ν is the kinematic viscosity of the fluid and D_x is the effective distance between the plates, i.e. the total distance between the planes of zero flow velocity. According to (20), the average velocity produced by the external force is

$$\bar{v}_z = \frac{gD_x^3}{12\nu}. \quad (21)$$

In our implementation $\bar{v}_z$ was straightforwardly estimated. This quantity corresponded to the time average of the z component of the center of mass velocity of the MPC cells, calculated over the whole simulated system.

In order to study the specific relationship between $\bar{v}_z$ and g produced by our algorithm, we carried out a set of experiments in which the external force per unit mass took 51 different values uniformly distributed in the range $g \in [0, 0.5]$. Notice that, in addition, these experiments were performed for the twelve values of the collision angle α, specified at the end of section III-B. This gives a total of 612 numerical experiments that were performed to test the applicability of the proposed technique.

In Fig. 2 we present the results of such experiments. For simplicity, there we have only included the results for some selected values of the collision angle, namely $\alpha = 15°, 45°, 75°, 105°, 135°, 165°$. It can be observed that for small values of the external force, all the experiments show that $\bar{v}_z$ increases linearly with g, as it is expected from (21). In Fig. 2 it is also shown that the linear relation between the average velocity and the external force is broken for large values of the latter, $g \gtrsim 0.4$. It should be stressed that although, for simplicity, this situation is illustrated in Fig. 3 only for the case $\alpha = 15°$, it is indeed observed for the complete set of numerical experiments. This implies that the proposed technique for confining MPC fluids might
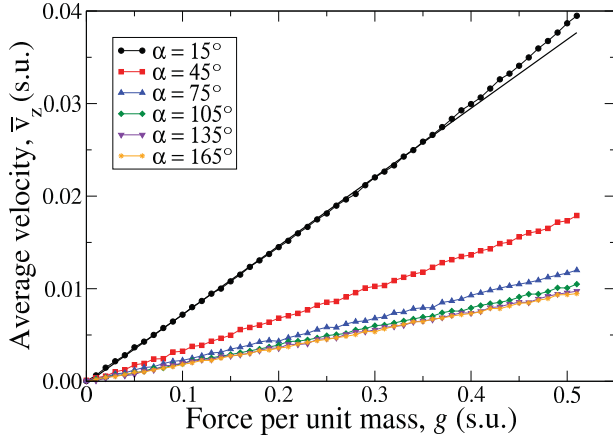
Fig. 2. Simulation results (symbols) for the average velocity induced by force fields with different magnitude in a MPC fluid confined by the force given by (7). The black line shown in the case $\alpha = 15°$ corresponds to a fit of the experimental data obtained from a simple least squares method.
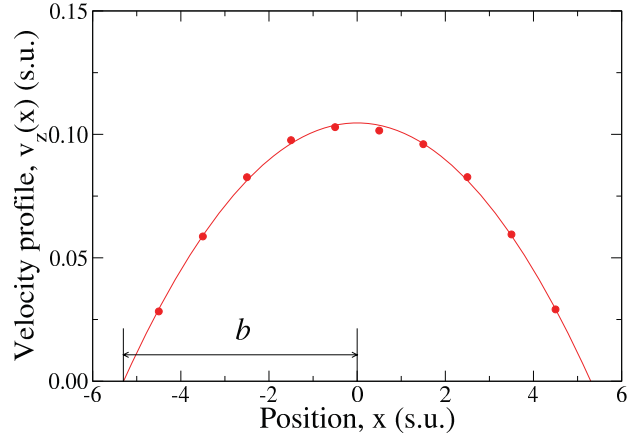

Fig. 3. Typical velocity profile obtained from the hybrid MD-MPC algorithm with confinement forces. Symbols correspond the results of simulations while the continuous curve has been obtained from a quadratic fit of the simulation data. The parameter b is used to estimate the value of D_x, as it is described in the main text.

lead to a stress tensor that depends on the external force, an effect that was already anticipated by the analysis carried out in section II-B. However, this effect is not significant if simulations are restricted to small values of the external force, and the model proposed in the present work could be used to simulate the flow of a confined fluid with a viscosity coefficient independent of the external force field.

It can be readily seen from (21) that the results presented in Fig. 2 could be used to estimate the viscosity coefficient of the simulated fluid as function of the collision angle. More precisely, the numerical results could be approximated by a linear fit, obtained e.g. by the method of least squares, and the slope obtained from such a fit for a given value of α, $s(\alpha)$, will yield the viscosity through

$$\nu = \frac{D_x^3}{12\, s(\alpha)}. \tag{22}$$

It is clear, however, that an independent estimation of the quantity D_x is required for this purpose.

The procedure that we used to estimate D_x is illustrated in Fig. 3. There, we present a typical velocity profile obtained from our simulation experiments, corresponding to the values $\alpha = 180°$ and $g = 0.2$. This profile was obtained as a time average of the z component of the center of mass velocity of the MPC cells, evaluated at different positions x inside the simulation cell. We notice firstly that this profile is parabolic, as it is expected from (20). In fact, the continuous line presented in Fig. 4 corresponds to a nonlinear fitting of the numerical results obtained by assuming a quadratic relation between v_z and x. The resulting value of the x coordinate in which the velocity profile is found to vanish, represented by the symbol b in Fig. 3, is used in our estimation of D_x. More precisely we have $D_x \simeq 2b$. Our numerical results show that variations of D_x with the external force field are not significant, but D_x depends strongly on the collision angle α. Thus, we obtain an estimation of the parameter D_x by fixing the value of α, and averaging the resulting values of b for the set of simulations performed with different external forces g.

Once this quantity has been determined, the effective viscosity produced by our specific implementation of MPC dynamics can be estimated by using (22).

We present in Fig. 4 the results obtained from this analysis, where the estimated viscosity of the MPC fluid was calculated for the different values of the collision angle used in our simulations. It can be observed from Fig. 4 that ν increases rapidly for small values of α, but it is stabilized and presents no significant variations for values of α close to $180°$. In addition, Fig. 4 shows that the proposed algorithm is able to simulate confined fluids whose viscosities can be tunned in a rather wide range of values by properly selecting the parameter α.

B. Velocity Profile

We will finally present an analysis of the detailed velocity profiles produced by our numerical implementation and resulting from the externally imposed forces and the confinement interaction with the walls. With this purpose, we carried out a comparison between the results of simulations and the classical Poiseuille formula, (20), in which we used the values of ν and D_x estimated according to the procedure described earlier in the preceding section IV-A. For brevity, here we will restrict ourselves to present this comparison for simulations carried out with three different collision angles $\alpha = 15°, 90°, 180°$, and three different values of the external force per unit mass $g = 0.1, 0.2, 0.4$. Such comparison is illustrated in Fig. 5, where it can be observed that the proposed model is satisfactory to describe the behavior of the simulated system.

It is interesting to notice that in our numerical implementation the distance D_x does not coincide with the location of the confining walls, i.e. $D_x \neq L_x$. This implies that the proposed algorithm simulates flows with partial slip at the boundaries, an effect that can be interpreted in terms of an apparent viscosity contribution at the neighborhood of
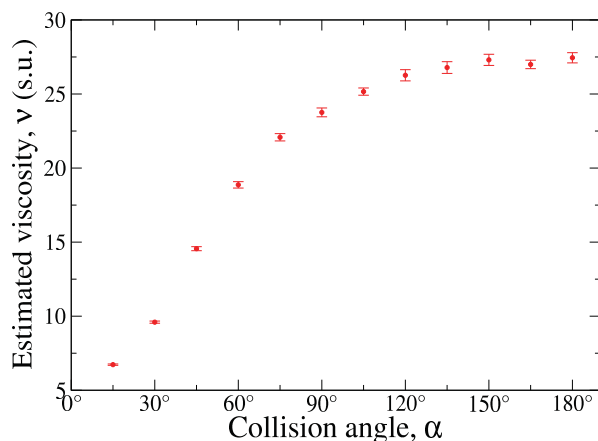
Fig. 4. Viscosity coefficient of the confined MPC fluid as function of the collision angle α. Symbols with error bars are the results from simulations.
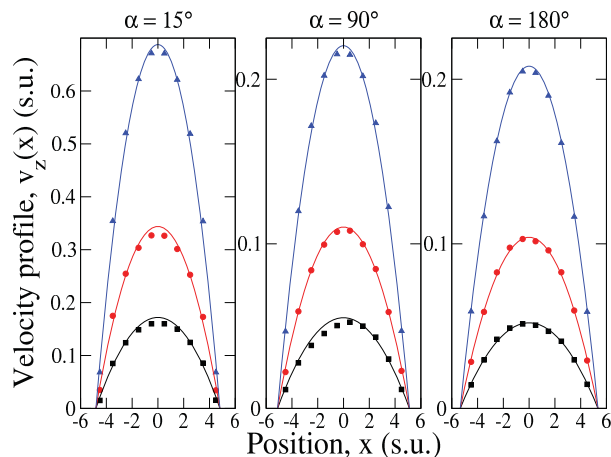

Fig. 5. Plane Poiseuille flows induced by the application of pressure gradients with different magnitudes $g = 0.1$ (black squares), $g = 0.2$ (red circles), and $g = 0.4$ (blue triangles), in simulations of confined MPC fluids.

the confining surfaces, as it was anticipated from the analysis carried out in section II-B. We found experimentally that for values of the collision angle in the range $\alpha \in [60°, 180°]$, $D_x > L_x$; while for smaller values of α, i.e. $\alpha \lesssim 60°$, D_x was found to be smaller than L_x. This indicates that in the regime where kinetic effects dominate, the force exerted by the confining surfaces makes the MPC fluid move in the opposite direction to the external force $\vec{g}$. This effect can be explained by noticing that when α is small, MPC particles may travel large distances without changing their velocities appreciably. Thus, particles well inside the simulation cell, with rather large velocities along the direction of $\vec{g}$, are able to collide with the wall, from where they are rejected with large velocities pointing mainly in the direction of $-\vec{g}$. These rejected particles drag the fluid at boundary walls and are responsible for the afore mentioned backward motion.

V. CONCLUSIONS

We have presented a new methodology for simulating solid-fluid interactions in MPC. The proposed technique is based on the introduction of an explicit interaction between the simulated fluid particles and the surface representing the solid wall. This interaction is summarized by (9), whose most important feature is that the microscopic details of the confinement wall have been averaged and reduced to its local geometrical properties. This characteristic of the proposed method could be used in order to generalize it with the purpose of making it able for simulating MPC fluids confined in more complex geometries, e. g. a mirror symmetric 3D channel.

We have tested the validity of the proposed model in simulations of a MPC fluid confined between two parallel planes and we have shown that the proposed method yields the correct velocity profile expected from hydrodynamics, when boundary conditions are of the slip type.

Modification of the present algorithm could be introduced that would allow the simulation of solid surfaces with arbitrary slip coefficient. These problems are under current research.

REFERENCES

[1] A. Malevanets and R. Kapral, *J. Chem. Phys.* **110** (1999) 8605
[2] A. Malevanets and R. Kapral, *J. Chem. Phys.* **112** (2000) 7260
[3] D. Frenkel and B. Smith, *Understanding Molecular Simulations: from Algorithms to Applications*, Academic Press, San Diego, 2002
[4] S. H. Lee and R. Kapral, *J. Chem. Phys.* **121** (2004) 11163
[5] N. Kikuchi, J. F. Ryder, C. M. Pooley and J. M. Yeomans, *Phys. Rev. E* **71** (2005) 061804
[6] J. T. Padding and A. A. Louis, *Phys. Rev. E* **74** (2006) 031402
[7] J. M. Yeomans, *Physica A* **369** (2006) 159
[8] E. Tüzel, M. Strauss, T. Ihle and D. M. Kroll, *Phys. Rev. E* **68** (2003) 036701
[9] T. Ihle and D. M. Kroll, *Phys. Rev. E* **63** (2001) 020201
[10] T. Ihle and D. M. Kroll, *Phys. Rev. E* **67** (2003) 066706
[11] C. M. Pooley and J. M. Yeomans, *J. Phys. Chem. B* **109** (2005) 6505
[12] G. Gompper, T. Ihle, D.M. Kroll and R.G. Winkler, *Adv. Polym. Sci.* **221** (2009) 1-87
[13] N. Kikuchi, A. Gent and J. M. Yeomans, *Eur. Phys. J. E* **9** (2002) 63
[14] A. Malevanets and J. M. Yeomans, *Europhys. Lett.* **52** (1999) 231
[15] M. Ripoll, K. Mussawisade, R. G. Winkler and G. Gompper, *Europhys. Lett.* **68** (2004) 106
[16] A. Lamura, G. Gompper, T. Ihle and D. M. Kroll, *Europhys. Lett.* **56** (2001) 319
[17] E. Allahyarov and G. Gompper, *Phys. Rev. E* **66** (2002) 036702
[18] H. Noguchi and G. Gompper, *Phys. Rev. E* **72** (2005) 011901
[19] A. Moncho Jordá, A. A. Louis and J. T. Padding, *Phys. Rev. Lett.* **104** (2010) 068301
[20] A. Moncho Jordá, A. A. Louis and J. T. Padding, *J. Chem. Phys.* **136** (2012) 064517
[21] M. Belushkin, R. G. Winkler and G. Foffi, *J. Phys. Chem. B* **115** (2011) 14263
[22] H. Híjar, *J. Chem. Phys.* **139** (2013) 234903
[23] J . K. Withmer and E. Luijten, *J. Phys.: Condens. Matter*, **22** (2010) 104106
[24] R. G. Winkler and C. C. Huang, *J. Chem. Phys.* **130** (2009) 074907
[25] J. P. Hansen and I. R. McDonald, *Theory of simple liquids*, 2nd ed. Academic Press, London, 1986
[26] H. Híjar and G. Sutmann, *Phys. Rev. E* **83** (2011) 046708
[27] L. D. Landau and E. M. Lifshitz, *Fluid Mechanics*, 2nd revised English version, Pergamon, London (1959)